Pergamon

Int. J. Heat Mass Transfer. Vol. 38, No. 10, pp. 1799–1811, 1995

0017-9310/95 $9.50+0.00

0017-9310(94)00296-7

Nucleate boiling on a thin heating plate: heat transfer and bubbling activity of nucleation sites

W. BERGEZ

15bis, rue du Professeur Martin, 31500 Toulouse, France

(*Received* 21 *September* 1994)

Abstract—Time-dependent aspects of nucleate boiling on a thin plate in well-wetted conditions have been studied for water at saturation, atmospheric pressure, and low heat flux by using simultaneous recordings of ebullition activity and wall temperature measured with a thermochromic liquid crystal. Existing heat transfer descriptions are not adequate in this case. Accounting for wall temperature variations leads to a new determination of the ebullition frequency and to a comprehensive but still non-predictive model of boiling heat transfer with two characteristic wall superheats, combining heat supply and activity of the nucleation site.

1. INTRODUCTION

Modelling heat transfer during nucleate boiling in the regime of isolated bubbles can be achieved by partitioning the surface into areas influenced and not influenced by nucleation sites, and where two different types of heat transfer take place. Such models are comprehensive in that they predict the total heat transfer from the contributions of different mechanisms which can enhance transfer compared to the single phase natural convection case. In this model, total heat flux is given by the addition of two terms [1]:

$$Q = (1-A)Q_C + AQ_B \quad (1)$$

where Q_C is the heat flux due to the natural convection in the presence of surrounding bubbles and applies to the area not influenced by a nucleation site, and Q_B is the boiling heat transfer corresponding, in the simplest model, to the contributions of the latent heat transport and the quenching effect after bubble departure [2]:

$$Q_B = \tfrac{4}{3}\pi R_D^3 \rho_V h_{fg} f \frac{n}{A} + 2k_L \sqrt{\frac{f}{\pi a_L}} \Delta T_W \quad (2)$$

where R_D and f must be considered as average values.

Four parameters of the nucleation site activity appear to play an important role: the nucleation site density n, the radius of bubbles at departure R_D, the frequency of bubble emission f, and the area of influence of a site n/A. Thus, the use of equations (1) and (2) for the prediction of the heat transfer requires the knowledge of how these parameters vary with boiling conditions. A very large number of experimental and theoretical data have been produced, resulting in new levels of modelling showing the complexity of nucleate boiling phenomenon.

1.1. *Active nucleation site density*

Brown [3] established a widely used correlation giving the number of active nucleation sites as a power function of the minimum cavity radius. This last quantity can be linked to the wall temperature through a thermodynamic nucleation criterion (complete review in ref. [4]). The resulting relations required empirical constants for each heating wall–fluid combination. Yang and Kim [5] produced a prediction of active site density in which the only input was the average cavity density measurable by a scanning electron microscope and a differential interference contrast microscope. As they pointed out, the heater roughness does not seem to be a relevant parameter in boiling. Wang and Dhir [6] gave experimental evidence showing that the active site density is very sensitive to the value of the contact angle.

1.2. *Volume of bubble at departure*

Numerous formula have been proposed to predict bubble size at departure. Models refer to a force balance at the end of the growth stage. Neglecting viscous drag and bubble inertia forces, departure occurs when the buoyancy force becomes larger than the contact and liquid inertia forces. It is likely that this event depends on the growth rate through the role of the inertia forces. The influence of growth rate on bubble departure typically appears indirectly through a common parameter, the Jakob number, Ja [7]. For a given fluid and pressure, and at saturation, this number is proportional to the wall superheat. Thus, in predictions including Ja, rate of bubble growth and size at departure depend directly on ΔT_W. Zeng *et al.* [8] introduced the bubble growth rate as the unique input in their model to predict R_D (apart from the external constraints such as pressure, gravity or Jakob number).

1.3. *Frequency of bubble emission*

Study of bubble emission frequency has led to descriptions of complex behaviour during boiling.

NOMENCLATURE

A ratio of boiling area to total area
a thermal diffusivity [$m^2 s^{-1}$]
c thermal capacity [$J kg^{-1} K^{-1}$]
d_W, d_{LC}, d_F wall, liquid crystal and polyester film thicknesses [m]
f ebullition frequency [s^{-1}]
h convective heat transfer coefficient [$W m^{-2} K^{-1}$]
h_{fg} latent heat of evaporation [$J kg^{-1}$]
Ja Jakob number
k thermal conductivity [$W m^{-1} K^{-1}$]
K ratio of area of influence to bubble projected area
n active nucleation site density [m^{-2}]
Nu Nusselt number
Q heat flux [$W m^{-2}$]
Q_B boiling heat flux [$W m^{-2}$]
Q_C convective heat flux [$W m^{-2}$]
r radius [m]
R_D bubble radius at departure [m]
Ra Rayleigh number
t time [s]
t_g bubble growth time [s]
t_w waiting time [s]
T temperature [K]
T_a activation temperature [K]
T_c cessation temperature [K]
T_m cavity mouth equilibrium temperature [K]
$\overline{T_W}$, $\Delta\overline{T_W}$ average temperature and superheat in the region surrounding a nucleation site [K]
T_{W0}, ΔT_{W0} average temperature and superheat of the cooled area at bubble departure [K]
ΔT superheat [K]
x axial co-ordinate [m]
X, X_0 non-dimensional axial co-ordinate.

Greek symbols
α non-dimensional coefficient [equations (A1)–(A4)]
β root of transcendental equations
δ liquid thermal layer thickness [m]
θ contact angle [rad]
Θ non-dimensional temperature
κ non-dimensional coefficient [equations (A1)–(A4)]
λ non-dimensional coefficient [equations (A1)–(A4)]
ρ density [$kg m^{-3}$]
τ non-dimensional time
ϕ heat flow at an active site [W].

Subscripts
L liquid
LC liquid crystal
V vapour
W wall
∞ bulk.

Hsu and Graham [9] proposed a model in which the waiting time between departure and next bubble growth is given by the transient heat conduction in the liquid thermal layer after departure. The role of cavity geometry and of meniscus motion was considered by several authors, some also accounting for heat conduction in the wall [4, 10]. Calka and Judd [11] and Sgheiza and Myers [12] gave experimental evidence for irregular activity at some sites. Eddington and Kenning [13] and Judd [14] concluded that vapour seeding possibly occurs when the base of a growing bubble from one site dried out above adjacent sites. Kenning [15] introduced a $T_a/\phi/T_c$ model, where T_a and T_c are temperatures of activation and cessation of nucleation of an active site, and ϕ is heat removal at this site whilst active. If ϕ exceeded the heat supply, the temperature of the site could vary around T_a and T_c which would result in irregular activity on a site. The possibility of more than two characteristic temperatures of a site was considered in [16]. In a similar approach, Pasamehmetoglu and Nelson [17] developed a numerical model for thermal interference between sites using a finite volume method to solve the three-dimensional heat conduction equation in the wall with boundary conditions on the fluid side derived from existing nucleate boiling formula. When the authors chose a random distribution of sites on the heating surface, they deduced that the activity of nucleation sites became chaotic and waiting time variations could reach 55%. Deligiannis and Cleaver [18] studied the interaction between sites by the action of a wave due to bubble growth on the activation of surrounding sites.

1.4. *Area of influence of a nucleation site*

Han and Griffith [19] suggested that the area of influence of an active site may be considered equal to the projected area of the liquid region perturbed by the rising bubble. This leads to an area of diameter twice the diameter of the sphere:

$$K = \frac{A}{n\pi R_D^2} = 4. \quad (3)$$

This result has been widely used and substantially modified to fit experimental data (for example $K = 1.8$

in ref. [2]). Del Valle and Kenning [20] took into account the possible overlap between areas of influence to correct the contribution of the quenching effect.

It appears that in the case where the boiling process is well defined by the averaged values of Q, ΔT_w, n, R_D, f and K, one can effectively find from equation (2) and the relations among these quantities a comprehensive prediction of how ΔT_w varies with Q. However, the above variables may be very sensitive to any variation of one among them. For example, as Kenning noted [16], the correlation of Brown [3] relates n to ΔT_w by a power factor 5; that is, a 5% uncertainty in wall superheat generates variations of 25% in active site density. This sensitivity among these variables shows the limitation of a stationary analysis as it can lead to large fluctuations of boiling variables. In this work, some aspects of the problem of time dependent variations of the wall superheat are examined for particular and somewhat extreme boiling conditions.

Most of the models contain explicitly or implicitly the assumption that the wall behaves as a perfect thermal conductor, its temperature being constant in space and time at given boiling conditions. However, it has long been known that the wall temperature varies locally by periodic drops which can reach 10 K [21, 22]. Raad and Myers [23] confirmed the existence of a cold spot under a growing bubble with the use of a liquid crystal which display colour changes in a narrow range of temperature (2 K). Sgheiza and Myers [12] found new evidence for wall temperature variations with an infrared camera operating in line-scan mode (1000 frames s^{-1}).

Several models of temperature variations during bubble growth have been proposed. Beer *et al.* [24] solved numerically the two-dimensional unsteady heat conduction equation in the wall around a site during bubble growth with a uniform transient heat flux on the fluid side boundary equal to the increase of latent heat in the bubble. In ref. [25] a large cooling effect beneath the growing bubble was predicted by modelling of the heat transfer during microlayer evaporation.

Heat transfer inside the wall has also been invoked to explain the irregular activity of nucleation sites. Eddington and Kenning [13] suggested that thermal interference between neighbour sites might explain cases of deactivation when the heat supply is increased, and, as noted above, Kenning [15] and Pasamehmetoglu and Nelson [17] found similarities to chaotic representations of site activity.

However, the role of the wall thermal properties directly implied in wall temperature variations is not yet fully elucidated. Although the extended examination of heat flow rate data in saturated nucleate pool boiling by Cooper [26] tends to show that the heater material has little effect on heat transfer, some studies appear to suggest otherwise. For example, Magrini and Nannei [27] found a dependency of heat transfer on the thermal properties and thickness of the wall.

An important advance was achieved by Kenning [28] in a work based on using thermochromic liquid crystal with a colour play range from 104 to 132°C. In a study of water boiling on a thin stainless steel plate at atmospheric pressure and heat flux of 100 kW m^{-2}, he developed temperature maps with variations from 4 to 30 K over distances of a few millimetres. Depending on the chemo-physical properties of the plate, the distribution of active nucleation sites could vary not only in density, but also in location (sites that should be active according to mechanistic nucleation criteria were not active) probably because of the sensitivity to the way sites are covered with liquid. This could invalidate the prediction of sites density based only on the surface topography and contact angle [4, 5]. Kenning concluded by advising prudence in using all existing models or measurement techniques of mean wall temperature that neglect spatial variations in wall superheat which can be expected on surfaces of heaters with moderate thermal conductivity.

The experimental study presented here was performed with the apparatus of Kenning [28], and interpretations are based on video recordings that he partly produced [29]. Liquid crystals are a very convenient means to investigate wall temperature variations due to their fast time response combined with the representation of two-dimensional information. Video recordings simultaneouslly provide information on wall temperature distribution and boiling activity. Wall temperature variations at an active site during the waiting period and their effect on boiling heat transfer are analysed.

2. EXPERIMENTAL METHODS

The boiling apparatus was designed by Kenning [28, 30] and used for ref. [31]. It consists of a small glass-sided rectangular aluminium cell ($46 \times 103 \times 100$ mm^3) where distilled water was boiling at atmospheric pressure and at saturation. The sides are insulated with silicon and each contains a heating cartridge, which allows saturated boiling at low heat flux. The bottom of the cell is a plate of aluminium with a hole (30×20 mm^2) under the boiling surface in order to have a view from below. The boiling surface (40×30 mm^2) is a strip of either (i) 0.125 mm thick stainless steel abraded with P600 grade emery paper or (ii) 0.075 mm thick brass with no abrasive treatment. Heat is supplied by electric current passing through two heavy copper electrodes soldered to the ends of the strips. Silicon rubber guaranteed the tightness of the whole assemblage.

The procedure given in ref. [30] to prepare the rear of the boiling surface was, first, to paint it with matt black enamel and to bake it in order to avoid contamination of the liquid crystal from solvents. An unencapsulated cholesteric liquid crystal was then applied by brushing, and covered with an optically

inactive 0.023 mm thick polyester film. This film provides protection and a more uniform liquid crystal thickness; in addition, the action of imposing a slight shear stress on it forces it into the planar texture in which it shows thermochromic properties. Layer thickness was estimated by measuring its weight on test samples; thicknesses were found to vary from 5 to 10 μm, which is in the lower range of values encountered for encapsulated liquid crystals.

The liquid crystal used in this experimental study was of the same sample as in refs. [28, 29], but the colour-active temperature range had decreased to 102–124°C, probably due to ageing [30, 31].

In order to record simultaneously boiling activity and colour variations at the rear of the heating plate, the incident light from a xenon flash was divided into two beams: one passed through the cell and lit the boiling surface, while the other lit the liquid crystal at an angle of 7° from the normal (Fig. 1). The resulting beams were collected on a high-speed colour video camera Nac 200 (200 frames s^{-1}), so that the upper half of the images exhibited the bubbling activity on the heating plate, while the lower half recorded the variations of colour of the liquid crystal. The resolution of the video camera allowed a spatial resolution on the images of 0.1 mm $pixel^{-1}$.

Calibration was done *in situ* with a hot air jet impinging on an aluminium plate put on the stainless steel plate. The temperature was measured with a thermocouple located at the base of the aluminium plate. The advantage of this method is that it allows direct calibration of the liquid crystal layer used in the experiments instead of a different reference layer which may display diffracted light with different intensities and saturation. But the method was not completely satisfactory because of heat transfer towards the copper electrodes. Conversion of colours into temperatures was done by eye with a maximum uncertainty of 2 K.

The heating surface was either (i) used with no special treatment (simply rinsed with "Decon 90" detergent then with water) which led to a rather poorly-wetted surface with a static contact angle for distilled water of the order of 60° or (ii) prepared first by rinsing with acetone, then scrubbing for 10 min with a solution of "Decon 90", rinsing with hot water, then with distilled water, which provided a well-wetted surface with a static contact angle on the order of 10°.

During the tests, recordings were done at different rates of heat supply ranging from 50 to 100 kW m^{-2}.

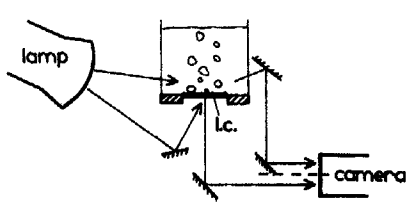

Fig. 1. Optical arrangements.

The images were examined either over a large number of sequences in order to obtain information on bubble departure diameters and waiting times, or frame by frame with photographic supports to obtain information on the correlation between ebullition cycle and variations of wall temperature. When the study was done directly on the video screen, tracing paper was used to locate the nucleation sites or measure the sizes of bubbles. On each photographic film, the sets of chosen sequences were systematically accompanied by the photographs of the calibration sequence to avoid any uncontrolled changes in the hues from the chemical treatment of film printing.

3. VIDEO RECORDINGS

3.1. *Boiling regimes*

Some of the features regarding the effects of wettability of the boiling surface on the nucleation site density and on the variations of the wall temperature already described by Kenning [28] were confirmed by the high-speed colour video recordings.

When no treatment of the surface was done (poorly-wetted surface), for a heat supply of 50 kW m^{-2}, the main characteristics were:

(1) approximately steady and uniform wall superheat of about 10 K with superimposition of red splashes;
(2) surface covered with nucleation sites;
(3) high frequencies of ebullition cycle (typically 50 Hz) and
(4) slow bubble growth rates and small bubble sizes at departure (growth time of about 10–20 ms for a departure diameter of about 1–2 mm).

When the surface was previously treated with the detergent (well-wetted conditions), for the same heat supply, the boiling characteristics changed as follows:

(1) the temperature pattern displayed large spatial and temporal variations (from 5 to 22 K superheat);
(2) the active sites at any time were very few and even zero on some frames if bubbles on the edge of the plate were not included;
(3) the frequency of bubble emission varied greatly from low values below 10 Hz up to the high values encountered for the poorly-wetted surface and
(4) most of the bubbles grew fast and their sizes at departure were large (of the order of 5 mm in diameter), with the exceptions of some sites producing small bubbles at high frequencies.

For the well-wetted surface, some further aspects could be examined on temperature variations occurring during the time of growth and the waiting period before a next growth.

3.2. *Boiling variables data*

3.2.1. *Bubble departure diameter.* In Fig. 2 the history of bubble growth and wall temperature variations is shown as obtained from a sequence of images taken during boiling on a stainless steel plate with a heat

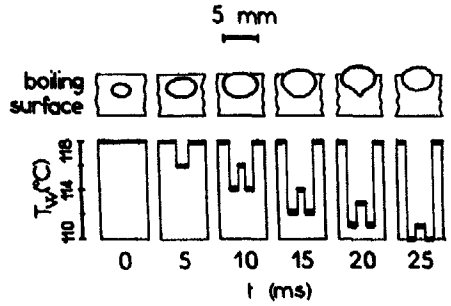

Fig. 2. History of wall temperature variations with bubble growth for a particular site.

flux of 50 kW m^{-2} and a liquid bulk temperature of 98°C. Bubble growth can be characterised by two stages: (1) the base of the bubble is growing at a rate close to that of the bubble radius (quasi hemispherical bubble), first two frames; (2) the base, after having reached a maximum radius, recedes till a neck forms, third and fourth frames, and the bubble starts to break off the surface, fifth frame. A similar description can be found in ref. [32].

Figure 3 shows two diagrams $R_D(t)$ for two different sites active during the same test (well-wetted stainless steel and heat flux of 50 kW m^{-2}). The bubble diameter at a nucleation site (here sites a or b) appears to vary greatly during the boiling process. Variations range ±25% for site a, ±15% for site b. There exists for given boiling conditions a large range of bubble departure diameters (factor 3 in Table 1), which can be linked to differences between growth rates at different sites. Generally, the growth took place during three to five frames, and a rough relation could be established between rate of growth and size at departure: small bubbles were departing at the second or third frame, while large bubbles were commonly departing at the fourth or fifth frame. However, exceptions were observed where a large bubble departed at the third frame. Accurate measurements of growth rate are not achievable with recordings at 200 frames s^{-1}. In the asymptotic isobaric growth model (bubble radius proportional to $t^{1/2}$), approximate estimations of the growth coefficient led to values between 0.01 and 0.03 m s$^{-1/2}$, for growth times varying from 15 to 20 ms, at constant boiling conditions [31].

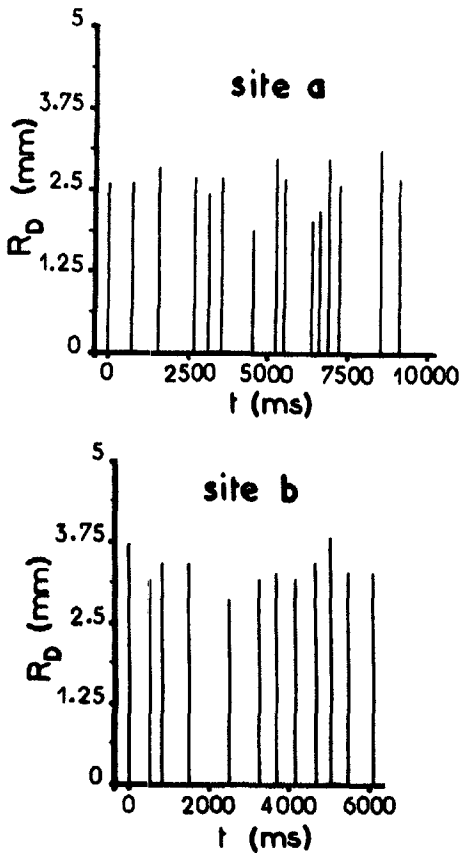

Fig. 3. $R_D(t)$ for two sites at the same boiling conditions.

Table 1. Characteristics of the six sites used in Fig. 6

Site number	Material	Wall thickness [μm]	Heat supply [kW m^{-2}]	Average R_0 value [mm]
1	Stainless steel	125	50	2.6
2				3.2
3				1.1
4				0.9
5	Brass	75	70	1.6
6				2.75

3.2.2. *Wall temperature variations at an active site.* The liquid crystal displayed a variation of colour at the second frame (Fig. 2) which corresponds to a slight cooling. In the third frame, the temperature generally decreased 8–10 K, but a hotter spot appeared in the centre region delimited by a circle approximately 1 mm in diameter. Due to delay of temperature change of the liquid crystal (Appendix A) and radial heat diffusion, the temperature–heat transfer data conversion was not adequate during bubble growth [31].

The cooling effect lasted up to bubble departure. After departure, if no bubble grew near the concerned site, the temperature of the cooled region reached again its initial value in a few hundred milliseconds. Table 2 shows this evolution for a site having produced a bubble at $Q = 50$ kW m^{-2}, with $R_D = 1.8$ mm.

3.2.3. *The ebullition frequency.* The frequency of ebullition cycle was very irregular for some sites (such

Table 2. Time variations of wall temperature at one site after bubble departure (well-wetted stainless steel, $Q = 50$ kW m^{-2}, $R_D = 1.8$ mm)

t [ms]	0	15	40	70	130
$T_w \pm 1$°C	107	111	112.5	114	116

as site a of Fig. 3), when for others (such as site b of Fig. 3) there were periods of few seconds where the site was quite regularly activated. Examination on the video recordings of the departure sizes of bubbles and the ebullition frequencies gives evidence of a dependency between these two quantities.

Response time to a temperature step change of the wall with the layer of liquid crystal and the polyester film as estimated in Appendix A is found to be very short compared to the waiting period. Consequently the wall may be considered infinitely thin in the analysis of heat transfer in the wall during the waiting period.

3.2.4. *The area of influence*. The area of the cooled region is slightly less than the projected area of the bubble at departure. It may correspond to the maximum radius of the bubble base which is approximately 80% of the departure diameter [31]. However, in the subsequent discussion this difference will be neglected and the cooled area will be confounded with the projected area of the bubble at departure.

4. ANALYSIS

The following analysis considers the behaviour of boiling variables for an isolated site existing in the well-wetted conditions and low heat flux case reported in the previous section.

4.1. *Variations of bubble departure diameter*

As noted above, the bubble diameter at departure changes significantly from one site to another (sometimes by a factor of three). A possible cause for these variations lies in variations of the maximum wall superheat at each site. This assumption leads to the following analysis.

The notion of activation temperature T_a and cessation temperature T_c for each site has been introduced by Kenning [15]. When wall temperature is smaller than T_a there is no nucleation at the site, and the heat transfer is purely convective. If the wall temperature reaches T_a, the site becomes active and produces successive ebullition cycles. The controlling temperature for bubble growth, and then for the cycle, is the temperature of nucleation corresponding to the initiation of each growth, which is equal to or less than T_a.

For illustration, the case of a re-entrant cavity with a conic mouth can be considered. For this case the liquid–vapour interface equilibrium curve is shown in Fig. 4. It represents the equilibrium temperature of the interface as a function of the volume of vapour trapped in the cavity, obtained from a thermodynamic relation for the equilibrium of a curved liquid–vapour interface plus a geometrical relation between the position of the meniscus and its curvature as in [4].

For such a site, there are three characteristic temperatures: the activation temperature T_a, the cessation temperature T_c and the outer mouth equilibrium temperature T_m. Initial nucleation is possible when the interface passes through the minimum radius of curvature at the inner mouth ($T > T_a$). At bubble detachment, a vapour embryo remains at the outer mouth and, depending on the quantity of heat removed during bubble growth, the temperature of the site T can be above or below T_c; if $T > T_c$, a subsequent growth can occur when $T > T_m$, or when the embryo at the mouth has its top in contact with a liquid at a temperature above T_m [9]. Otherwise, if $T < T_c$, and neglecting delay in heat and mass transfer, the interface reaches instantaneously a position of equilibrium at the inner mouth. The site then nucleates again if $T > T_a$.

When the wall is well-wetted, the activation and cessation temperatures may be large. Then, at initial nucleation the growth rate is high and at departure the bubble is large. It follows that the cooling due to bubble growth is efficient enough to reduce the site temperature below T_c. A next growth will be possible when the wall temperature at the site again reaches T_a which means repeated high growth rates and large departure diameters. As the activation temperature is a property of the site geometry, then it is possible that the local maximum wall superheat might vary from one site to another which could explain the differences in bubbles sizes at departure. This hypothesis is discussed further below.

It must be emphasized that these arguments greatly simplify the real boiling phenomenon. It appears in fact that the bubble departure size can be quasi regular for some sites and irregular for others, as is shown in Fig. 3.

4.2. *Wall temperature variations*

Due to heat diffusion in the wall and the liquid crystal (Appendix A), it is very difficult to convert the variations of the temperature distribution at the rear of the wall during bubble growth into data on the wall temperature and the boiling heat transfer (independently of errors in the colour to temperature conversion). However, it is possible to find contributions to these variations. It has already been shown [25] that the evaporation of a microlayer at the base of the bubble could produce the annular cooled region under the growing bubble observed on the video recordings. To complete the description of heat removal from the wall during the entire growth, an attempt was made [31] to consider the stage when the bubble base recedes. Results were not conclusive because of too many unknown parameters.

As noted in the previous section, it is possible to consider the wall as infinitely thin during the time elapsed from bubble departure to next bubble growth. Then, the temporal variations of the wall temperature may be obtained from

$$\rho_w c_w \frac{\partial T_w}{\partial t} = -\frac{h}{d_w}(T_w - T_\infty) + \frac{Q}{d_w} + k_w \frac{1}{r}\frac{\partial}{\partial r}\left(r\frac{\partial T_w}{\partial r}\right) \quad (4)$$

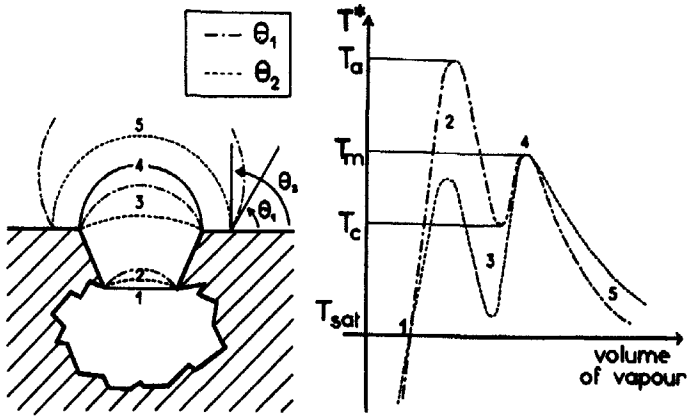

Fig. 4. Equilibrium curve of the vapour–liquid interface for a re-entrant cavity with two values of contact angle θ.

where the thermal capacity of the liquid crystal and polyester film layers have been neglected. h is the convective heat transfer coefficient. The initial conditions are:

$$\text{for } t = 0 \quad \begin{matrix} r < R_D & T_W = T_{W0} \\ r > R_D & T_W = \overline{T_W} \end{matrix}$$

where T_{W0} is the initial temperature of the cooled area assumed uniform and $\overline{T_W}$ is the surrounding wall temperature. Equation (4) may be investigated with the help of experimentally observed temperature evolution from a video recording sequence. Data in Table 2 are used for this purpose with $\overline{T_W}$ estimated at 120 ± 1°C. It is possible to estimate roughly in equation (4) the relative contribution of the three different kinds of heat transfer: convective heat transfer, heat supply and radial heat conduction (Appendix B). This analysis indicates that radial heat conduction is the major term. Assuming that the heat supply and convective heat transfer terms balance each other, equation (4) simplifies to

$$\rho_W c_W \frac{\partial T_W}{\partial t} = k_W \frac{1}{r} \frac{\partial}{\partial r}\left(r \frac{\partial T_W}{\partial r}\right). \tag{5}$$

To account for the constancy of wall temperature beyond $r = R_D$ observed in the video recordings, a boundary condition of $T_W = \overline{T_W}$ at $r = R_D$ is now imposed; the initial conditions are unchanged. Equation (5) is then integrated to give at $r = 0$ [33]

$$T_W = \overline{T_W} - 2(\overline{T_W} - T_{W0}) \sum_{n=1}^{\infty} \frac{\exp(-\beta_n^2 a_W t / R_D^2)}{\beta_n J_1(\beta_n)} \tag{6}$$

where (β_n) are the positive roots of $J_0(\beta) = 0$. J_0 and J_1 are Bessel functions of order 0 and 1. Equation (5) fits the data quite well (Fig. 5). To account for uncertainties in the measured wall temperature in equation (6), the curve for $\overline{T_W} = 120$°C is enclosed by two curves representing maximum error of $\overline{T_W} - T_{W0}$ (13 ± 2 K).

In conclusion, for a situation of boiling with low contact angle and low heat flux, an isolated nucleation site acts as a heat sink during bubble growth, possibly due to the evaporation of a microlayer at the base of the bubble which requires a large rate of heat removal. Before a subsequent nucleation occurs, the site is reheated by heat transfer in the wall. Radial heat conduction from the surrounding superheated region of the wall is possibly the primary control during this period, the major part of heat supply being dissipated through convective transfer to the liquid. This conclusion has important implications for determination of the waiting time.

4.3. *The waiting time*

A dependency between bubble sizes at departure and ebullition frequency or waiting time (growth time being neglected here) was proposed 30 years ago [34]. The proposal is based on the idea that after bubble departure subsequent bubble growth will occur only when the liquid thermal layer is re-established. It can be deduced intuitively that the required time for this re-establishment increases with increasing volume of the liquid region where the thermal layer is perturbed. This region may be related to the volume of the bubble at departure. It leads to the result that fR_D^3 is constant

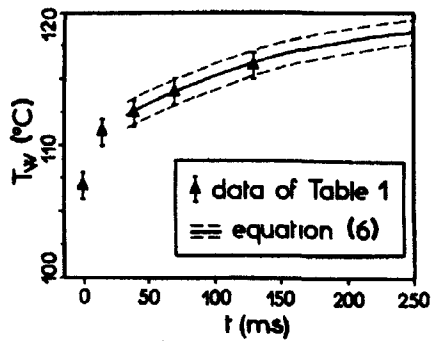

Fig. 5. Wall temperature variations during the waiting period.

for a given heat flux. However, the models based on the re-establishment of the liquid thermal layer predict small values for the waiting times (of the order of 10–20 ms for saturated water at atmospheric pressure [19]), and so are not appropriate for the case of low ebullition frequencies.

If one considers the evolution of temperature as analysed above, and still assuming that a site nucleates when its temperature is above an activation temperature, one can infer that a subsequent growth will occur after bubble departure when the wall temperature again reaches the activation temperature (T_a or T_m for the simple cavity considered previously). Then, assuming that reheating is controlled mainly by radial heat conduction, the waiting time can be related to a heat diffusion time scale, that is R_D^2/a_W. From equation (6), the temperature is re-established at approximately $0.95(\overline{T_W}-T_{W0})$ when [25, 31]

$$t=\frac{1}{\beta_1^2}\ln\left(\frac{1}{0.05\beta_1 J_1(\beta_1)}\right)\frac{R_D^2}{a_W}\approx\frac{R_D^2}{2a_W} \tag{7}$$

where β_1 is the first positive root of $J_0(\beta)=0$. Thus, a theoretical waiting time can defined by the relation

$$t_w=\frac{R_D^2}{2a_W}. \tag{8}$$

Figure 6 presents the experimental results obtained for six different sites characterised in Table 1. Equation (8) is followed quite well. This confirms that heat supply may not have a significant role during reheating because it balances the convective heat transfer in equation (4). When the growth time t_g is negligible relative to the waiting time, then the ebullition frequency follows the equation

$$fR_D^2=\frac{R_D^2}{t_g+t_w}\approx 2a_W. \tag{9}$$

A relation of this type has already been proposed by Rohsenow [7]:

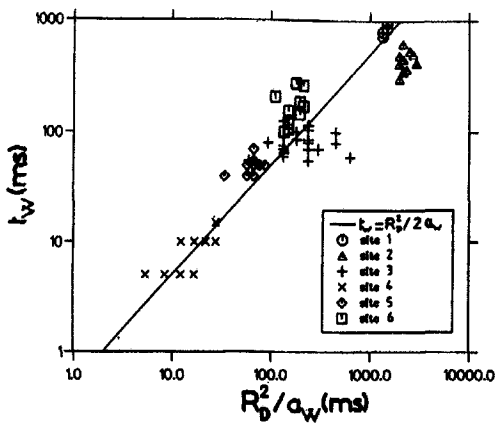

Fig. 6. Waiting time variations with R_D^2/a_W for six sites at two different boiling conditions defined in Table 2.

$$R_D\sqrt{f}=\tfrac{3}{8}\sqrt{\pi a_L}\,Ja.$$

In this relation, the product fR_D^2 depends on the liquid properties and the wall temperature. This is a consequence of a model of bubble growth in a transient temperature field due to quenching, and so is similar to the analysis of Hsu and Graham [9] mentioned above. In contrast, equation (9) has the distinction of being independent of wall temperature or heat flux in the conditions studied here.

If in general this tendency is verified, there may be very large discrepancies between the measured waiting time and the value predicted by equation (8) (Fig. 3). A first possible cause is that the site may have more than three characteristic temperatures that depend on the geometry of the cavity (a proposition made in ref. [16]). This would make the history of the position of the interface, as developed in the previous section, more complicated, and possibly make the following activation occur at a temperature below $\overline{T_W}$. A similar argument is the possible existence of two or more adjacent sites simultaneously active and so close together that the bubbles grow virtually at the same place. Those sites may have different characteristic temperatures and the order in which they nucleate may have no particular frequency. A third explanation is the possible existence of interference between sites by heat conduction in the wall, as mentioned in the introduction [15, 17].

4.4. *Area of influence of a nucleation site*

The video recordings provide new evidence for the cooling effect of the bubble growth that was mentioned in [23, 32]. Furthermore, the cooled area appears to coincide with the projected area of the bubble at departure, as noted above. This result makes the determination of the area of influence of a nucleation site quite problematic—if K is defined in this manner and not as a correlation constant fit to experimental data. On one hand, a hydrodynamic prediction based on the wake flow of a rising sphere shows that convective effects may take place over a region twice the diameter of the sphere, and on the other hand there is no particular sign of enhanced heat transfer beyond the projected area of the growing bubble. Furthermore, Lee and Nydhal [35] found from a numerical solution of the Navier–Stokes and energy equations during bubble growth and departure, that the thermal layer is affected by bubble departure only in a region immediately beneath the bubble with a maximum effect at the centre. This result suggests that the transient heat conduction in the thermal layer cannot be integrated over a region larger than πR_D^2 ($K=1$).

The above analysis of heat transfer during the waiting time shows the role of the radial heat transfer. The corresponding radius of penetration by heat diffusion at the end of the waiting period can be given by $\sqrt{4a_W t_w}$. From equation (8), we can then estimate the

penetration radius as $1.5R_D$. Considering that this radius can be interpreted as the radius of an area influenced by the nucleation site, on the basis of heat transfer inside the wall, we have $K = 2$.

Thus, from the present results, not taking into account the possibility of enhanced convective heat transfer, the area of influence is estimated to be confined to a diameter 1.5 times the bubble departure diameter, although the heat transfer during the bubble growth and possibly the quenching effect occur in a limited area underneath the bubble.

5. CONSEQUENCE ON HEAT TRANSFER AND BUBBLING ACTIVITY

From the above considerations, one can infer some consequences for the relation between boiling heat transfer and bubbling activity in the well-wetted condition and at low heat flux. The analysis now concerns a boiling cell delimited by the area of influence, and therefore is a region different from the cooled region considered in the heat transfer model above.

5.1. *Heat balance at an active site*

The enhancement of heat transfer appears to take place in a well defined region confined under the bubble and mainly during a short period corresponding to bubble growth. It can be attributed to the latent heat transport mechanism in which high heat transfer is caused by the evaporation of a liquid microlayer at the base of the bubble. Although small in magnitude when integrated over the whole cycle, this contribution is of primary importance as the cause of large temperature variations.

In equation (2) the quenching effect is modelled by the sudden contact of the superheated wall with cooler liquid resulting in transient heat conduction in the liquid. However, the associated thermal layer thickness varies as $\sqrt{\pi a_L t}$, while the liquid thermal layer thickness varies as $1.65k_L/h$ for water at atmospheric pressure [36]. This implies that the quenching effect will not last the entire waiting time, and will be replaced by convective effects after some 10 ms. The quenching term in equation (2) then is overestimated because it is integrated over the complete ebullition period. To more precisely evaluate the quenching effect, the assumption of transient heat conduction over a semi-infinite region is replaced with a region limited by the convective thermal layer thickness, with zero initial liquid superheat, and boundary conditions defined as $\Delta T_L = 0$ at $x = 0$ and $\Delta T_L = \Delta T_W$ at $x = \delta$, where $\delta = k_L/h$ is taken as the thickness of a linear thermal layer [9]. The liquid superheat is given by (from ref. [4])

$$\frac{\Delta T_L}{\Delta T_W} = \frac{x}{\delta} + \frac{2}{\pi}\sum_1^\infty \frac{\cos n\pi}{n} \exp\left(-n^2\pi^2 \frac{a_L t}{\delta^2}\right) \sin\left(n\pi \frac{x}{\delta}\right). \tag{10}$$

The corresponding heat flux at the wall is therefore

$$Q = k_L \left.\frac{\partial T_L}{\partial x}\right|_\delta = \frac{k_L \Delta T_W}{\delta}\left[1 + 2\sum_1^\infty \exp\left(-n^2\pi^2 \frac{a_L t}{\delta^2}\right)\right]. \tag{11}$$

Integrating this relation over the waiting period gives the energy per surface area conducted into the liquid during this period:

$$\int_0^{t_w} Q\,dt = \frac{k_L \Delta T_W}{\delta} t_w + \frac{\rho_L c_L \delta \Delta T_W}{3} - 2\rho_L c_L \delta \Delta T_W \sum_1^\infty \frac{1}{n^2\pi^2} \exp\left(-n^2\pi^2 \frac{a_L t_w}{\delta^2}\right). \tag{12}$$

The first term of the right-hand side is the convective heat transfer; the addition of the second and third terms represents the enhancement of heat transfer due to the quenching effect. In the case of a long waiting time ($a_L t_w/\delta^2 > 1$), the third term can be neglected and the contribution of the quenching effect is given by the ratio of the first two terms:

$$\frac{\text{convective effect}}{\text{quenching effect}} = \left(\frac{k_L \Delta T_W}{\delta} t_w\right)\left(\frac{\rho_L c_L \delta \Delta T_W}{3}\right)^{-1} = 3\frac{a_L t_w}{\delta^2}. \tag{13}$$

In this evaluation the quenching effect contribution appears to depend on the bubbling frequency which leads to less enhancement in the heat transfer at low frequency.

For the complete cycle a balance may be written between rate of heat supply Q, latent heat transport, quenching effect and convection heat transfer. The area of influence of the nucleation site is the quantity defined as above, that is $K = 2$, and the quenching effect is assumed to occur over this entire area. The balance is given with the help of relation (8) by the following equation:

$$Q = \frac{2}{K}\rho_v h_{fg} \sqrt{a_w}\sqrt{t_w f^2} + h\Delta T_W\left(t_w f + \frac{\delta^2}{3a_L} f\right). \tag{14}$$

This relation provides information on the variation of wall superheat with the heat supply. Unfortunately the interpretation of ΔT_W is not direct; it is a characteristic superheat for the quenching and convective phase. A better model should contain at least the two extreme temperatures of the ebullition cycle. This can be approximated by identifying ΔT_W with the mean value of the maximum and minimum superheats of the cycle. The convective heat transfer coefficient is not very sensitive to wall superheat (see Appendix B) so is still evaluated assuming the surrounding region is controlled by natural convection: $h = Q/\Delta T_w$. The resulting heat balance can be then written as

$$Q = \frac{2}{K}\rho_v h_{fg}\sqrt{a_w}\sqrt{t_w f^2} + \frac{Q}{\Delta\overline{T_w}}\frac{\Delta\overline{T_w}+\Delta T_{w0}}{2}\left(t_w f + \frac{k_L\rho_L c_L}{3}\frac{\Delta\overline{T_w}^2}{Q^2}f\right). \quad (15)$$

For the conditions of Table 2, this equation yields 7.5 kW m^{-2} for the latent heat transport and 49 ± 7 kW m^{-2} for the quenching and convective effects. The 15% uncertainty in the last contribution is due to uncertainty in the colour to temperature conversion. This result compares with the heat supply of 50 kW m^{-2}, which is quite compatible considering the experimental uncertainties.

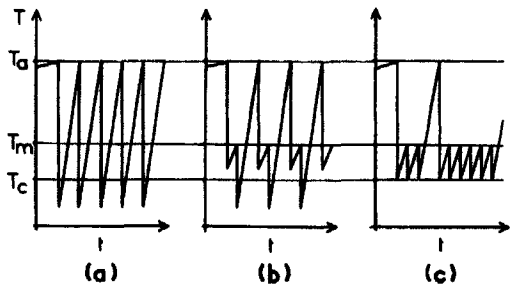

Fig. 7. Schematic representation of site temperature variations derived from combination of equation (15) with site characteristics.

5.2. *Bubbling activity*

For an activated isolated site equation (15) imposes a condition of regular nucleation activity on its boiling properties. A balance exists between heat removal by boiling Q_B [right term of (15)] and heat supply Q. One limit is no nucleation, that is f and $(\Delta\overline{T_w} - \Delta T_{w0})$ are 0. In theory, as R_D depends on the wall superheat and the heat supply as well as ΔT_{w0}, equation (15) is an implicit relation between Q and $\Delta\overline{T_w}$ independent of the geometry and the chemo-physical properties of the site.

For an isolated site with characteristic temperatures T_a, T_c and T_m, when heat supply is increased, there will be a time at which the wall temperature reaches the activation temperature through free convection regimes. The condition implied by equation (15) is that the wall superheat at a site oscillates between T_a ($= \overline{T_w}$) and T_{w0}, which implies that there is no net heat transfer enhancement compared to single phase heat transfer; however, as proposed above, if $T_{w0} > T_c$, the site can nucleate at T_m before T_a is reached again. At this point, equation (15) implies that: ft_w and h are almost constant and, because the difference $(\Delta\overline{T_w} - \Delta T_{w0})$ is increasing with $\Delta\overline{T_w}$, the characteristic quenching superheat (evaluated as the mean value of $\Delta\overline{T_w}$ and ΔT_{w0}) can be considered to vary slowly also. Then, in contrast to equation (2) or even (14), equation (15) shows that, in the expression of Q_b, the only term that changes rapidly is f. If the site nucleates at $T_m < T_a$, the corresponding frequency will increase and yield $Q_b > Q$. The average wall superheat $\Delta\overline{T_w}$ decreases and the site reaches a new equilibrium cycle at $\overline{T_w} = T_m$, which implies that nucleation enhances heat transfer.

This model can lead to a large number of possible site temperature histories and bubbling activities. In the simple case of a site with three characteristic temperatures, depending on the difference between T_{w0} and T_c, the bubbling activity can change as shown in Fig. 7. When T_{w0} is well below T_c, the site is in a stable regime of bubble production [Fig. 7(a)]. If in the second cycle T_{w0} falls below T_c, the site cannot reach a stable regime of bubble production but oscillates between two regimes [Fig. 7(b)]. When the difference between T_{w0} and T_c is very small, a slight change in ebullition conditions can 'switch off' the site: the regime is intermittent [Fig. 7(c)].

If the site cavity has more than three characteristic temperatures, wall temperature variations would be more complicated and at times not periodic at all. As the number of characteristic temperatures increases, their mutual differences decrease. If these differences diminish to the order of variations of T_{w0} due to the sensitivity of this quantity to locally unsteady bubbling conditions, this quantity can be considered as undetermined. In this case, the following very schematic representation of site activity can be proposed.

Given a set of decreasing activation–cessation temperatures $(T_a[i], T_c[i])$ we can define a set of 'transitions' $T_a[i] \rightarrow T_c[j]$ which means that if the nucleation occurs at $T_a[i]$ the minimum wall temperature T_{w0} falls around $T_c[j]$. Then depending on the position of T_{w0} relative to $T_c[j]$, there are two possibilities: $T_c[j] < T_{w0}$, then the next nucleation occurs at $T_a[j+1]$ (transition $T_c[j] \rightarrow T_a[j+1]$); or, $T_c[j] > T_{w0}$, then the next nucleation occurs at $T_a[j]$ (transition $T_c[j] \rightarrow T_a[j]$). This simple model of variations in wall temperature at a nucleation site introduces a random process which leads to an unpredictable behaviour of the site. However, it includes necessarily unsteady influences on the cell that can affect the bubble growth (such as convective effects).

Thus, without considering the possibility of site interactions, the combination of constraints on the heat balance at the boiling cell [equation (15)] and the geometric and chemo-physical properties of the site leads to a description of complex but periodic variations of the maximum and minimum wall superheat. Intermittence or completely unpredictable activity of the site may be the result of uncontrolled influences from the region surrounding the site which make T_{w0} undetermined.

5.3. *Limitations of the model*

The above model has been established for an isolated site at particular boiling conditions: low contact angle, low heat flux, thin plate and moderate thermal conductivity of the wall. If the contact angle is increased, activation temperatures decrease and, for a given site, equation (15) predicts lower and less vari-

able wall temperatures with higher ebullition frequencies. It means that the classical description of equation (2) might be applicable. This is the case of the poorly-wetted surface in the video recording data reported here.

These data show that the model of heat transfer described by equation (15) is correct up to maximum heat flux values of 100 kW m^{-2}. The limitation comes from two effects; frequency increases and active sites become too numerous to be considered as isolated. This results in some equilizing of wall temperatures. At present, it is not possible to predict how an increase in the heat supply in the limit of the model would modify the heat balance.

In the case of a thick wall where the transverse temperature gradient cannot be neglected ($d_W \geqslant \sqrt{a_W t_g}$), the situation is different. First, large distortion by heat diffusion makes the liquid crystal technique proposed by refs. [28, 30] inadequate to characterise boiling heat transfer. Secondly, the heat transfer is controlled by different boundary conditions. It was shown in refs. [25, 31] that wall temperature variations at the boiling surface might still exist due to rapid bubble growth. But for the reheating phase, there is competition between axial and radial heat diffusion which may affect significantly determination of the waiting time. However, a comprehensive model should include the existence of two extreme wall superheat for an ebullition cycle, as in equation (15).

When thermal conductivity of the wall increases the cooling effect of bubble growth becomes less significant [31]. The wall temperature distribution tends to be uniform and the ebullition frequency increases, so the classical description of equation (2) is correct. Experimental constraints on thickness and electrical resistance of the wall rendered it generally impossible to study the effect of thermal conductivity. For boiling surfaces with k ranging from the values for stainless steel to values for brass, large wall temperature variations may exist.

Further limiting parameters such as system pressure, subcooling or change of fluid were not explored because of limitations of the experimental technique.

6. CONCLUSIONS

The ebullition of water at low heat flux has been studied at atmospheric pressure and at saturation on a thin plate made of stainless steel or brass. Analysis of wall temperature and bubbling activity data that were obtained simultaneously indicate that the existing boiling heat transfer models are not applicable. Boiling variables were studied accounting for the wall temperature variations. A simple model of heat conduction in the wall suggests a new prediction of the waiting time, equation (8), which fits experimental data quite well.

Heat balance on a boiling cell was also considered. The variations of wall superheat were included in this balance with a crude hypothesis for an equivalent temperature for the quenching phase [equation (15)]. Relating the boiling properties of an isolated active nucleation site and the heat supply allowed an analysis of site activity, and provided a new implicit condition combining heat transfer considerations and geometric and chemo-physical properties of the cavity. Intermittence or chaotic behaviour can be explained on the basis of this model for a cavity with a complex geometry for which site activity parameters are very sensitive to local unsteady change in boiling conditions. Further improvements in understanding and prediction require additional experimental data.

Acknowledgement—This work is partly the result of doctoral research, the experimental part of which was performed in the laboratory of Dr D. B. R. Kenning of Oxford University, to whom I am very grateful for the helpful materials he generously provided.

REFERENCES

1. B. B. Mikic and W. M. Rohsenow, A new correlation of pool data including the effect of heating surface characteristics, *ASME J. Heat Transfer* **91,** 245–250 (1969).
2. R. L. Judd and K. S. Hwang, A comprehensive model for nucleate pool boiling heat transfer including microlayer evaporation, *ASME J. Heat Transfer* **98,** 623–629 (1976).
3. W. T. Brown Jr., A study of flow surface boiling, Ph.D. Thesis, Massachusetts Institute of Technology, Cambridge, Massasuchetts (1967).
4. R. Cole, Boiling nucleation. In *Advances in Heat Transfer* (Edited by J. P. Hartnett and T. F. Irvine), Vol. 10, pp. 85–166. Academic Press, New York (1974).
5. S. R. Yang and R. H. Kim, A mathematical model of pool boiling nucleation site density in terms of the surface characteristics, *Int. J. Heat Mass Transfer* **31,** 1127–1135 (1988).
6. C. H. Wang and V. K. Dhir, Effects of the surface wettability on active nucleation site density during pool boiling of water on a vertical surface, *Proceedings of the 28th National Heat Transfer Conference*, HTD-Vol. 159, pp. 89–96, ASME, New York (1991).
7. W. M. Rohsenow, Boiling. In *Handbook of Heat Transfer* (Edited by W. M. Rohsenow and J. P. Hartnett), Section 13. McGraw-Hill, New York (1973).
8. L. Z. Zeng, J. F. Klausner and R. Mei, A unified model for the prediction of bubble detachment diameters in boiling systems—I. Pool boiling, *Int. J. Heat Mass Transfer* **36,** 2261–2270 (1993).
9. Y. Y. Hsu and R. W. Graham, An analytical and experimental study of the thermal boundary layer and the ebullition cycle in nucleate boiling, NASA TN-D-594 (1961).
10. A. Singh, B. B. Mikic and W. M. Rohsenow, Effect of superheat and cavity size on frequency of bubble departure in boiling, *ASME J. Heat Transfer* **99,** 246–249 (1977).
11. A. Calka and R. L. Judd, Some aspects of the interaction among nucleation sites during saturated nucleate boiling, *Int. J. Heat Mass Transfer* **28,** 2331–2342 (1985).
12. J. E. Sgheiza and J. E. Myers, Behaviour of nucleation sites in pool boiling, *A.I.Ch.E. Jl* **31,** 1605–1613 (1985).
13. R. I. Eddington and D. B. R. Kenning, The prediction of flow boiling populations from gas bubble nucleation experiments. *Proceedings of the 6th International Heat Transfer Conference*, Vol 1, pp. 275–280, Toronto (1978).

14. R. L. Judd, On the nucleation site interaction, *ASME J. Heat Transfer* **111,** 747–751 (1989).
15. D. B. R. Kenning, Wall temperature in nucleate boiling: spatial and temporal variations, *Proceedings of the 9th Heat Transfer Conference*, Vol 3, pp. 33–38, Jerusalem (1990).
16. D. B. R. Kenning, Wall temperature variations and the modelling of bubble nucleation sites, *Proceedings Engineering Foundation Conference on Pool and External Flow Boiling*, pp. 105–109, Santa Barbara, ASME (1992).
17. K. O. Pasamehmetoglu and R. Nelson, Cavity-to-cavity interaction in nucleate boiling: the effect of heat conduction within the heater, *Proceedings of the 28th National Heat Transfer Conference, A.I.Ch.E. Symp. Ser.* **87**(283), 342–351 (1991).
18. P. Deligiannis and J. W. Cleaver, Influence of surrounding bubbles on the rate of nucleation, *Int. J. Heat Mass Transfer* **36,** 3697–3701 (1993).
19. C. Y. Han and P. Griffith, The mechanism of heat transfer in nucleate pool boiling—I and II, *Int. J. Heat Mass Transfer* **8,** 905–914 (1965).
20. H. Del Valle M. and D. B. R. Kenning, Subcooled flow boiling at high heat flux, *Int. J. Heat Mass Transfer* **28,** 1907–1920 (1985).
21. F. D. Moore and R. B. Mesler, The measurement of rapid surface temperature fluctuations during nucleate boiling of water, *A.I.Ch.E. Jl* **7,** 620–624 (1961).
22. M. G. Cooper and A. J. P. Lloyd, The microlayer in nucleate boiling pool, *Int. J. Heat Mass Transfer* **12,** 895–913 (1969).
23. T. Raad and J. E. Myers, Nucleation studies in pool boiling on thin plates using liquid crystals, *A.I.Ch.E. Jl* **17,** 1260–1261 (1971).
24. H. Beer, P. Burow and R. Best, Bubble growth, bubble dynamics, and heat transfer in nucleate boiling, viewed with a laser interferometer. In *Heat Transfer in Boiling* (Edited by E. Hahne and U. Grigull), Chap. 2. Academic Press/Hemisphere, Washington (1977).
25. W. Bergez and A. Giovannini, Heat transfer in heating wall during microlayer evaporation in nucleate boiling, *Proceedings 28th National Heat Transfer Conference*, HTD-Vol. 159, pp. 81–87, ASME, New York (1991).
26. M. G. Cooper, Heat flow rates in saturated nucleate pool boiling—a wide-ranging examination using reduced properties. In *Advances in Heat Transfer* (Edited by J. P. Hartnett and T. F. Irvine), Vol. 16, pp. 157–239. Academic Press, New York (1984).
27. U. Magrini and E. Nannei, On the influence of the thickness and thermal properties of heating walls on the heat transfer coefficients in nucleate pool boiling, *ASME J. Heat Transfer* **97,** 173–178 (1975).
28. D. B. R. Kenning, Wall temperature patterns in nucleate boiling, *Int. J. Heat Mass Transfer* **35,** 73–85 (1992).
29. D. B. R. Kenning, Pool boiling on a thin horizontal plate, OUEL video, Oxford University (1991).
30. D. B. R. Kenning, Liquid crystal thermography as a tool for investigating the development of boiling, *Proceedings of the Engineering Foundation Conference on Pool and External Flow Boiling*, pp. 79–82, Santa Barbara, ASME (1992).
31. W. Bergez, Etude des transferts thermiques en régime d'ébullition stagnante et par nucléation dans la paroi chauffante, these, ENSAE, Toulouse, France (1991).
32. P. S. Roberts, The influence of wall thermal properties on bubble dynamics and heat transfer in nucleate boiling, Ph.D. Thesis, Oxford University (1984).
33. H. S. Carslaw and J. C. Jaeger, *Conduction of Heat in Solids* (2nd Edition), p. 198. Clarendon Press, Oxford (1959).
34. C. J. Rallis and H. H. Jawurek, Latent heat transport in saturated nucleate boiling, *Int. J. Heat Mass Transfer* **7,** 1050–1068 (1964).
35. R. C. Lee and J. E. Nydhal, Numerical calculation of bubble growth in nucleate boiling from inception through departure, *ASME J. Heat Transfer* **111,** 475–479 (1989).
36. T. E. Lippert and R. S. Dougall, A study of the temperature profiles measured in the thermal sublayer of water, Freon 113 and methyl alcohol during pool boiling, *ASME J. Heat Transfer* **90,** 347–352 (1968).
37. M. N. Özişik, *Heat Conduction*, p. 294. Wiley (1980).

APPENDIX A

To interpret the liquid crystal temperature data, it is necessary to have an idea of the delay time due to heat diffusion in the wall and the liquid crystal. As is noted in [28], the response of a liquid crystal when its molecular structure does not change (no transition from nematic to isotropic phase), is mainly controlled by its thermal properties. The delay of the liquid crystal to changes in the distance between the planes of molecules is negligible. Thus, one can estimate the response time from the transient response of the three layers of material (plate, liquid crystal and polyester film) from a temperature step change at the boiling surface (a detailed frequency response analysis is not needed at this point because the ebullition frequency is some orders lower than the characteristic time of heat diffusion in the wall).

The heat production term in the plate has no role if the initial temperature is a steady distribution with heat production. In addition, the properties of the liquid crystal and polyester film can be considered as identical. So the problem is reduced to the heat conduction into two slabs in perfect contact, one end being thermally isolated (on the film side) and the other end being at zero temperature; temperature is initially uniform and equal to unity.

The heat conduction equations for the response of the wall to a temperature step change at one end can be written with non-dimensional variables as follows:

$$\begin{gathered}\tau = 0 \quad \Theta_W = \Theta_{LC} = 1\\ \tau > 0 \quad \Theta'_{W_\tau} = \Theta''_{W_{XX}}\\ \Theta'_{LC_\tau} = \alpha\Theta''_{LC_{XX}}\\ X = -\lambda \quad \Theta'_{LC_X} = 0\\ X = 0 \quad \kappa\Theta'_{LC_X} = \Theta'_{W_X} \quad \text{and} \quad \Theta_W = \Theta_{LC}\\ X = 1 \quad \Theta_W = 1\end{gathered} \tag{A1}$$

where $\tau = a_W t/d_W^2$, $\lambda = (d_{LC}+d_F)/d_W$, $\alpha = a_{LC}/a_W$ and $\kappa = k_{LC}/k_W$. The solution can be found in form of series of orthogonal functions as proposed by Özişik [37]. At the interface of the liquid crystal and the polyester film ($X = X_0 = -d_{LC}/d_W$), the solution is

$$\Theta_{LC}(X_0) = \sum_1^\infty e^{-\beta_n^2\tau}\frac{\Psi_{LC_n}(X_0)}{N_n}\left(\frac{\kappa}{\alpha}\int_{-\lambda}^0 \Psi_{LC_n}\,dX + \int_0^1 \Psi_{W_n}\,dX\right) \tag{A2}$$

with

$$\begin{aligned}\Psi_{LC_n}(X) &= -\tan\beta_n\cos\frac{\beta_n X}{\sqrt{\alpha}} + \frac{\sqrt{\alpha}}{\kappa}\sin\frac{\beta_n X}{\sqrt{\alpha}}\\ \Psi_{W_n}(X) &= -\tan\beta_n\cos\beta_n X + \sin\beta_n X\\ N_n &= \frac{\kappa}{\alpha}\int_{-\lambda}^0 \Psi_{LC_n}^2\,dX + \int_0^1 \Psi_{W_n}^2\,dX\end{aligned} \tag{A3}$$

and where (β_n) are the roots of

$$\left(1+\frac{\kappa}{\sqrt{\alpha}}\right)\cos\left[\beta\left(1+\frac{\lambda}{\sqrt{\alpha}}\right)\right] + \left(1-\frac{\kappa}{\sqrt{\alpha}}\right)\cos\left[\beta\left(1-\frac{\lambda}{\sqrt{\alpha}}\right)\right] = 0. \tag{A4}$$

The results, obtained when taking all the roots $\beta_n < 20$, are presented in Fig. 8 for two different thicknesses of the wall and of the liquid crystal. Choosing the temperature Θ_{LC} at the interface with the polyester film is a slight simplification, because the colour displayed by the liquid crystal corresponds to the superposition of dominant wavelengths due to Bragg's diffraction when the distance between molecular planes varies along the temperature gradient. According to our estimation of the value of the liquid crystal layer thickness (5–10 μm), its temperature should follow the boiling surface temperature with a delay of around 10 ms in the experiments. Observation of the first colour change on the video recording in the second frame shows that the liquid crystal does respond rapidly, in agreement with results of Fig. A1.

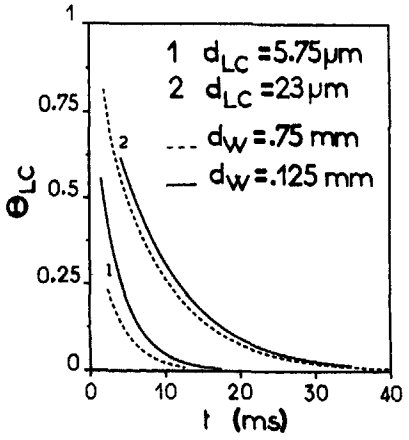

Fig. A1. Time response of the liquid crystal to a step change of boiling surface temperature (effect of wall and liquid crystal thicknesses) stainless steel wall.

APPENDIX B

The order of magnitude of the terms in equation (4) can be very roughly estimated. Equation (4) can be written with non-dimensional variables:

$$\frac{\partial\Theta}{\partial\tau} = -\frac{R_D^2 h}{d_W k_W}\left(\Theta + \frac{T_{W0}-T_\infty}{\overline{T_W}-T_{W0}}\right) + \frac{R_D^2}{d_W}\frac{Q}{k_W(\overline{T_W}-T_{W0})} + \Delta\Theta \quad \text{(B1)}$$

where $\Theta = (T_W - T_{W0})/(\overline{T_W} - T_{W0})$, $\tau = a_W t/R_D^2$ and Δ is the Laplace operator. Since for free convection $Nu \propto Ra^{1/3}$, one can assume that the heat transfer coefficient varies insignificantly during reheating. Estimating h at the end of the cycle, $h = Q/\Delta\overline{T_W}$, so $h \approx 2.3\,\text{kW m}^{-2}\,\text{K}^{-1}$ (data of Table 2). Then, with the boiling conditions of Table 2, we have $R_D^2 h/k_W d_w \approx 6$ and $(R_D^2/d_W(Q/k_W(\overline{T_W}-T_{W0}) \approx 10$. The addition of heat supply and convective heat transfer terms yields non-dimensional values varying from 6 to 0 during transient heat transfer. On the other hand, a characteristic of the diffusion process is to respond to a non-homogeneous distribution by rapid variations in non-dimensional variables (mathematically infinite at $r = R_D$). That means that $\Delta\Theta$ is, on average over the cooled region, larger than the two other terms by several orders of magnitude during a certain period. This consideration can be taken as an argument to neglect the heat supply and the convective heat transfer as being of the same order and balancing each other, but requires verifications on the basis of the results it gives. This was done in ref. [31] where it was shown that equation (4) without the diffusion term greatly underestimates the rate of wall temperature re-establishment.